**THE MARTIAN BOULDER AUTOMATIC RECOGNITION SYSTEM: COMPARISON TO OLD AND NEW TOOLS FOR LARGE-SCALE AUTOMATIC BOULDER MEASUREMENT**

D. R. Hood (Don_Hood@baylor.edu)[1], R. C. Ewing[2], S. Karunatillake[3], S. F. Sholes[4], C. I. Fassett[5], P. James[1,1]Baylor University Department of Geosciences, Waco, TX, [2]Texas A&M Department of Geology and Geophysics, College Station, TX, [3]Louisiana State University Department of Geology and Geophysics, Baton Rouge, LA, [4]Jet Propulsion Laboratory, California Institute of Technology, Pasadena, CA [5]NASA Marshall Space Flight Center, Huntsville, AL

**Introduction:** Meter-scale boulders are nearly ubiquitous on the martian surface and present both an immediate obstacle for exploration [1,2] as well as potential targets for scientific investigation [3,4,5]. However, measuring boulders manually is time-consuming and limits the scope of boulder investigations to small areas or transects where boulder morphometry can be assessed within a reasonable timeframe. To carry out large-scale (10s of $km^2$) investigations into boulder morphometry and distributions, we have developed the Martian Boulder Automatic Recognition System (MBARS) [6] as an open-source tool designed specifically to estimate boulder morphometry on the martian surface. Here, we present MBARS as it will be publicly released in 2022 and compare it to other boulder-estimation techniques: The Golombek-Huertas (G-H) method [1] and the Nagle-McNaughton (N-M) method [3]. We also present a technique for calibrating MBARS with manual boulder measurement.

**Dataset and Technique:** Images from the High-Resolution Imaging Science Experiment (HiRISE) instrument provide ~25-30 cm/pixel images and are widely spread over the martian surface. Boulders in these images generally appear as bright objects casting distinct shadows (Fig. 1), and the geometry of these shadows is used to determine the boulder size.

Boulders have been detected and measured from their shadows in prior work [1] for simultaneous estimates of both boulder height and width. MBARS applies the same fundamental concepts with a refined boulder shape model and different shadow fitting techniques.

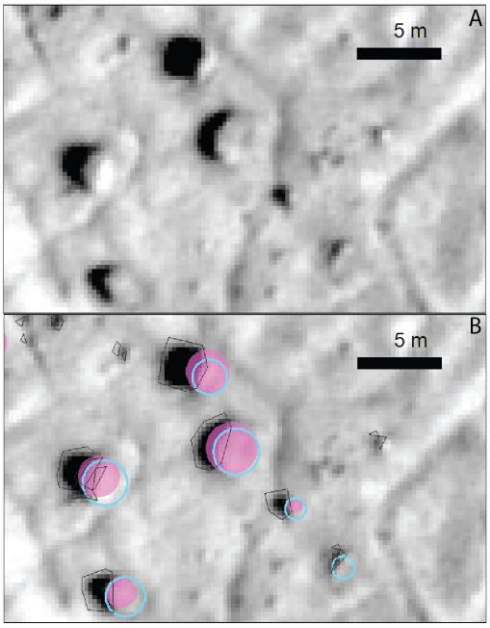


*Figure 1. Boulders in Area B (Fig. 3). (B) shows boulder outlines from manual measurement (blue), MBARS (pink), and the N-M conservative results (black polygons).*

**Automatic Boulder Detection:** Fig. 2 gives a flowchart view of our algorithm. As shown

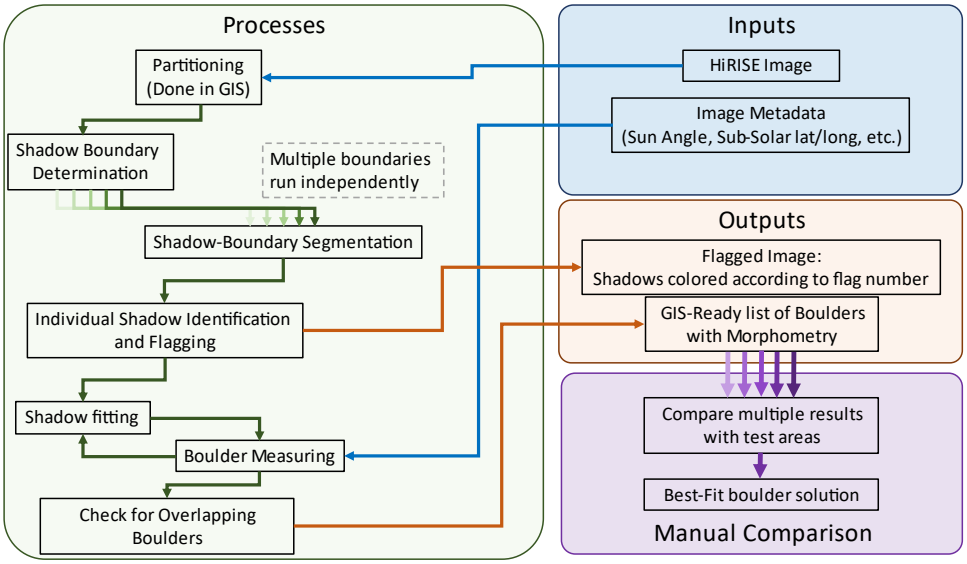


*Figure 2. Flowchart for MBARS. Using the inputs (blue box) MBARS analyzes the image using several shadow boundary estimations, each producing a unique output (orange box). These outputs are then compared against manual boulder estimates within test areas (purple box). The best fit across several areas is chosen as the final result.*

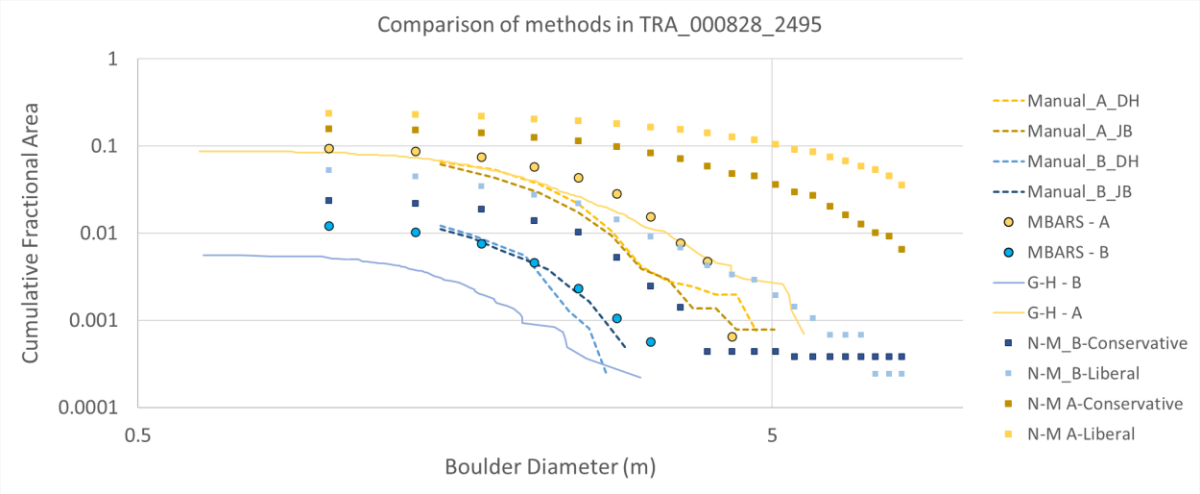


*Figure 3. Comparison of MBARS results (circles), G-H method results (solid lines), N-M method results (squares), and manual results (dashed lines) in test areas A (yellow) and B (blue). G-H method results and definitions of areas A and B were taken from prior publications [1]. Manual results were taken by two users, D. Hood (DH) and J. Brothers (JB).*

in the green box of Fig. 2, the first steps separate the HiRISE image into smaller partitions and calculate the shadow brightness boundary. We model the expected brightness of boulder shadows in the image, providing a different solution for each image. Depending on the model parameters, this modeled brightness will vary, and so multiple values for the shadow boundary are calculated and used independently. Using the shadow boundary value, image partitions are segmented, and individual shadows are identified. Based on both our boulder shape model, and the geometry of the HiRISE observation, the boulder width and height are determined from the width and length of the shadow.

**Calibration to Manual Results**: To calibrate MBARS and choose the optimal shadow brightness boundary, we select areas in each image in which boulders are measured manually to act as calibration points. Test areas are chosen to sample the range of boulder density in each image to ensure that the algorithm is accurate over all ranges. Surface albedo can also strongly impact the contrast of boulder shadows, impacting the shadow brightness model. To accommodate this, images with areas of both light and dark soil have separate test areas, and results are considered separately for these areas.

**Comparison to Prior Methods:** HiRISE image TRA_000828_2495 (Fig. 1) presents an optimal example to compare these algorithms. This area in the northern plains has low relief, an abundance of boulders, and estimates of the boulder population were made in prior publications [1]. We manually counted boulders in areas previously highlighted as having high (area A) and medium (area B) rock abundance [1], applied MBARS to this image, and carried out the N-M method [3] on the image to compare among the four methods (Fig. 1,3).

The manual results are shown in Fig. 3 as dashed lines of varying colors. Two datasets were generated for each test area independently by two users, demonstrating manual segmentation uncertainties. In area B MBARS results match most closely with manual results. Alternative methods either underestimate (G-H) or overestimate (N-M). In area A, the N-M method again overestimates the boulder abundance. MBARS and the G-H methods are comparable in this area, though both are overestimates of the manually measured boulder abundance.

These results indicate that the N-M method is poorly suited to these regions, likely due to the generally low boulder-soil contrast. Comparitively, MBARS and the G-H method produce results more consistent with manual measurement, though the G-H method is not available as an implemented tool. Upon release this year, MBARS will be the only open-source and most acessible tool to automatically assess boulder populations with minimal manual measurement required.

**Acknowledgments:** This work is funded by NASA's MDAP program, grant #80NSSC21K1093.

**References: [1]** Golombek, M. P., et al. (2008). *JGR*. doi: 10.1029/2007JE003065 **[2]** Golombek, M. P., et al., (2012). *The Mars Journal*. doi: 10.1555/mars.2012.0001 **[3]** Nagle-McNaughton, et al., (2020). *JARS*. doi: 10.1117/1.JRS.14.014522 **[4]** Levy, J. S., et al. (2021). *PNAS*, doi: 10.1073/pnas.2015971118 **[5]** Krishna, N., & Senthil Kumar, P. (2016) *Icarus*. doi: 10.1016/j.icarus.2015.09.033 **[6]** Hood, D. R., et al., (2018). *49th LPSC*. Abstract #2437